Space-Time Crystal and Space-Time Group

Shenglong Xu[1,2] and Congjun Wu[1]
[1]Department of Physics, University of California, San Diego, California 92093, USA
[2]Condensed Matter Theory Center and Department of Physics, University of Maryland, College Park, Maryland 20742, USA

(Received 24 August 2017; revised manuscript received 29 December 2017; published 27 February 2018)

Crystal structures and the Bloch theorem play a fundamental role in condensed matter physics. We extend the static crystal to the dynamic "space-time" crystal characterized by the general intertwined space-time periodicities in $D+1$ dimensions, which include both the static crystal and the Floquet crystal as special cases. A new group structure dubbed a "space-time" group is constructed to describe the discrete symmetries of a space-time crystal. Compared to space and magnetic groups, the space-time group is augmented by "time-screw" rotations and "time-glide" reflections involving fractional translations along the time direction. A complete classification of the 13 space-time groups in one-plus-one dimensions ($1+1$D) is performed. The Kramers-type degeneracy can arise from the glide time-reversal symmetry without the half-integer spinor structure, which constrains the winding number patterns of spectral dispersions. In $2+1$D, nonsymmorphic space-time symmetries enforce spectral degeneracies, leading to protected Floquet semimetal states. We provide a general framework for further studying topological properties of the $(D+1)$-dimensional space-time crystal.

DOI: 10.1103/PhysRevLett.120.096401

The fundamental concept of crystal and the associated band theory based on the Bloch theorem lays the foundation of condensed matter physics. Studies on the crystal symmetry and band structure topology have led to the discoveries of topological insulators, topological superconductors, and Dirac and Weyl semimetal states [1–3]. Periodically driving further provides a new route to engineering topological states—even in systems originally topologically trivial in the absence of driving—as explored in irradiated graphene [4,5], semiconducting quantum wells [6], dynamically modulated cold atom optical lattices [7], and photonic systems [8,9]. The periodicity of the quasienergy enriches the topological band structures [10–12], such as dynamically generated Majorana modes [13], 1D helical channels [14], and anomalous edge states associated with a zero Chern number [15,16]. Topological classifications for interacting Floquet systems have also been investigated [17–21].

For periodically driven crystals, most studies treat the temporal periodicity separately from the spatial one. In fact, the driven system can exhibit much richer symmetry structures than a simple direct product of spatial and temporal symmetries. In particular, a temporal translation at a *fractional* period can be combined with the space group symmetries to form novel space-time intertwined symmetries, which, to the best of our knowledge, have not yet been fully explored. For static crystals, the intrinsic connections between space-group symmetries and physical properties, especially topological phases, have been extensively studied [22–29]. Therefore, it is expected that the intertwined space-time symmetries could also protect nontrivial properties of the driven system, regardless of the microscopic details.

In this Letter, we propose the concept of a "space-time" crystal exhibiting the intertwined space-time symmetries, whose periodicities are characterized by a set of $D+1$ independent basis vectors, generally space-time mixed. A situation involving separate spatial and temporal periodicities is a special case and is also included. The full discrete space-time symmetries of space-time crystals form a class of new group structures—dubbed the space-time group, which is a generalization of a space group that includes "time-screw" and "time-glide" operations. A complete classification of the 13 space-time groups in $1+1$D is performed, and their constraints on band structure winding numbers are studied. In $2+1$D, 275 space-time groups are classified. Nonsymmorphic space-time symmetry operations, similar to their static space-group counterparts, lead to protected spectral degeneracies for driven systems, even when the instantaneous spectra are gapped at any given time.

Space-time crystal.—We consider the time-dependent Hamiltonian $H=P^2/(2m)+V(\mathbf{r},t)$ in $(D+1)$-dimensional space-time. $V(\mathbf{r},t)$ exhibits the intertwined discrete space-time translational symmetry as

$$V(\mathbf{r},t)=V(\mathbf{r}+\mathbf{u}^i,t+\tau^i), \qquad i=1,2,\ldots,D+1, \quad (1)$$

where $(\mathbf{u}^i,\tau^i)=a^i$ is a set of the primitive basis vectors. In general, the space-time primitive unit cell is not a direct product between the spatial and temporal domains. There may not even exist spatial translational symmetry at any

given time t, or temporal translational symmetry at any spatial location $\mathbf{r}$. Consequently, the frequently used time-evolution operator of one period for the Floquet problem generally does not apply. The reciprocal lattice is spanned by the momentum-energy basis vectors $b^i = (\mathbf{G}^i, \Omega^i)$ defined through $b^i \cdot a^j = \sum_{m=1}^{D} G_m^i u_m^j - \Omega^i \tau^j = 2\pi\delta^{ij}$. The $(D+1)$-dimensional momentum-energy Brillouin zone (MEBZ) may also be momentum-energy mixed.

Generalized Floquet-Bloch theorem.—We generalize the Floquet and Bloch theorems for the time-dependent Schrödinger equation $i\hbar\partial_t\psi(\mathbf{r},t) = H(\mathbf{r},t)\psi(\mathbf{r},t)$. Because of space-time translation symmetry, the lattice momentum-energy vector $\kappa = (\mathbf{k}, \omega)$ remains conserved. Only the κ vectors inside the first MEBZ are nonequivalent, and those outside the zone are equivalent up to integer reciprocal lattice vectors. The Floquet-Bloch states labeled by κ take the form of

$$\psi_{\kappa,m}(\mathbf{r},t) = e^{i(\mathbf{k}\cdot\mathbf{r}-\omega_m t)} u_m(\mathbf{r},t), \tag{2}$$

where m marks different states sharing the common κ value. $u_m(\mathbf{r},t)$ processes the same space-time periodicity as $H(\mathbf{r},t)$ and is expanded as $u_m = \sum_B c_{m,B} e^{i(\mathbf{G}\cdot\mathbf{r}-\Omega t)}$, with $B = (\mathbf{G}, \Omega)$ taking all the momentum-energy reciprocal lattice vectors. The eigenfrequency ω_m is determined through the eigenvalue problem defined as

$$\sum_{B'} \{[\varepsilon_0(\mathbf{k}+\mathbf{G}) - \Omega]\delta_{B,B'} + V_{B-B'}\} c_{m,B'} = \omega_m c_{m,B}, \tag{3}$$

where $\varepsilon_0(\mathbf{k})$ is the free dispersion and V_B is the momentum-energy Fourier component of the space-time lattice potential $V(\mathbf{r},t)$. The dispersion based on Eq. (3) is represented by a D-dimensional surface in the MEBZ which is a $(D+1)$-dimensional torus.

Dispersion winding numbers.—The band structure of the space-time crystal exhibits novel features that differ from those of the static crystal. For simplicity, below we use the $1+1$D case for an illustration. The dispersion relation $\omega(k)$ forms closed loops in the 2D toroidal MEBZ, each of which is characterized by a pair of winding numbers $\mathbf{w} = (w_1, w_2)$. Compared to the static case in which the band dispersion winds only around the momentum direction, here $\omega(k)$ is typically not single valued, and its winding patterns are much richer. The dispersions in the limit of a weak space-time potential $V(x,t)$ with a rhombic MEBZ are illustrated in Figs. 1(a) and 1(b), with details presented in Sec. I of the Supplemental Material (SM) [30]. When folded into the MEBZ, the free dispersion curve $\varepsilon_0(k)$ can cross at general points, not just on high symmetry ones. A crossing point corresponds to two equivalent momentum-energy points related by a reciprocal vector G. When $V_G \neq 0$, the crossing is avoided by forming a gap at the magnitude of $2|V_G|$. The total number of states for each $\mathbf{k}$ value is independent of the strength of $V(x,t)$; hence, crossing can only split along the ω direction and $d\omega/dk$ is always finite. Consequently, trivial loops with the winding numbers (0,0) are forbidden. Generally, the winding directions of the dispersion loops are momentum-energy mixed. Furthermore, different momentum-energy reciprocal lattice vectors can cross each other, leading to composite loops winding around the MEBZ along both directions, as shown in Fig. 1(b). Hence, in general, all patterns (w_1, w_2) are possible except for contractible loops.

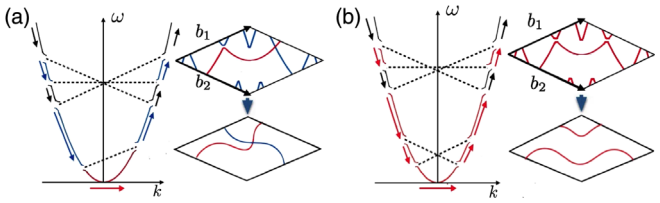

FIG. 1. Folding the band dispersions of the $1+1$D space-time crystal into the first rhombic MEBZ in the weak lattice limit. The momentum-energy reciprocal lattice vectors of nonzero V_B values are represented by dashed lines. The low-energy part of the free dispersion curve evolves to closed loops. (a) Two loops with the winding numbers $\mathbf{w_r} = (1,0)$ (the red curves) and $\mathbf{w_b} = (0,1)$ (the blue curves). (b) An extra nonzero V_G value connects two loops in (a), forming a new one with $\mathbf{w} = \mathbf{w_r} + \mathbf{w_b}$.

Space-time group.—To describe the symmetry properties of the $D+1$ dimensional space-time crystals, we propose a new group structure, dubbed a space-time group, defined as the discrete subgroup of the direct product of the Euclidean group in D spatial dimensions and along the time direction $E_D \otimes E_1$. Please note that, in general, the space-time group cannot be factorized as the direct product between discrete spatial and temporal subgroups. It includes not only space and magnetic group transformations in D spatial dimensions but also operations involving fractional translations along the time direction. Since space and time are nonequivalent in the Schrödinger equation, space-time rotations are allowed only in the twofold case.

To be concrete, a general space-time group operation Γ on the space-time vector $(\mathbf{r},t)$ is defined as

$$\Gamma(\mathbf{r},t) = (R\mathbf{r} + \mathbf{u}, st + \tau), \tag{4}$$

where R is a D-dimensional point-group operation, $s = \pm 1$ and $s = -1$ indicate time reversal, and $(\mathbf{u},\tau) = \sum_i m_i a^i$ represents a space-time translation with m_i values that are either integers or fractions. If $\tau = 0$, Γ is reduced to a space group or magnetic group operation according to $s = \pm 1$, respectively. If $\tau \neq 0$, when $(\mathbf{u},\tau)$ contains fractions of a^i, new symmetry operations arise due to the dynamic nature of the crystal potential, including the time-screw rotation and time-glide reflection, which are a spatial rotation and a reflection followed by a fractional time translation, respectively. The operation of Γ on the Hamiltonian is defined as $\Gamma^{-1}H(\mathbf{r},t)\Gamma = H[\Gamma(\mathbf{r},t)]$ and $\Gamma^{-1}H(\mathbf{r},t)\Gamma = H^*[\Gamma(\mathbf{r},t)]$ for $s = \pm 1$, respectively. Correspondingly,

the transformation M_Γ on the Bloch-Floquet wave functions $\psi_\kappa(\mathbf{r},t)$ is $M_\Gamma\psi_\kappa = \psi_\kappa[\Gamma^{-1}(\mathbf{r},t)]$ and $\psi^*_\kappa[\Gamma^{-1}(\mathbf{r},t)]$ for $s=\pm 1$, respectively.

Now we present a complete classification of the $1+1$D space-time groups. Because of the nonequivalence between the spatial and temporal directions, there are no square and hexagonal space-time crystal systems. The point-group-like operations are isomorphic to D_2, including reflection m_x, time reversal m_t, and their combination m_xm_t, i.e., the twofold space-time rotation. Consequently, only two space-time crystal systems are allowed—oblique and orthorhombic. There exist two types of glide reflections: the time-glide reflection, g_x, and g_t, denoted as "glide time reversal," which is time reversal followed by a fractional translation along the x direction.

The above $1+1$D space-time symmetries give rise to 13 space-time groups, in contrast to the 17 wallpaper space groups characterizing the 2D static crystals. The oblique Bravais lattice is simply monoclinic, while the orthorhombic ones include both primitive and centered Bravais lattices. The monoclinic lattice gives rise to two different crystal structures with and without twofold space-time axes, whose space-time groups are denoted by $P_{1,2}$, respectively, as shown in Fig. 2(a). For the primitive orthorhombic lattices, the associated crystal structures can exhibit the point-group symmetries m_x and m_t, and the space-time symmetries g_t and g_x. Their combinations give rise to eight space-time crystal structures, denoted as Pm_x, Pm_t, $P2m_xm_t$, Pg_x, Pg_t, $P2g_xg_t$, $P2m_xg_t$, and $P2g_xm_t$, respectively, as shown in Fig. 2(b). Four of them possess the twofold space-time axes, as indicated by the 2s in their symbols. For the centered orthorhombic Bravais lattices, three crystal structures exist, with their space-time groups denoted as Cm_x, Cm_y, and $C2m_xm_t$, respectively, as shown in Fig. 2(c). They all exhibit glide-reflection symmetries, and the last one possesses the twofold space-time axes as well. Two unit cells are plotted for the centered lattices to show the full symmetries explicitly, and their primitive basis vectors are actually space-time mixed.

The classifications of the space-time groups in higher dimensions are generally complicated. A general method is the group cohomology presented in Sec. II of the SM [30]. Specifically, a classification of the $2+1$D space-time group is outlined in Sec. III of the SM [30], in which the space-time group's structures are further enriched by spatial rotations and time-screw rotations. Compared to the 3D static crystals, the cubic crystal systems are not allowed, and two different monoclinic crystal systems appear with a perpendicular axis along the time and spatial directions, respectively. In total, there are seven crystal systems and 14 Bravais lattices, but 275 space-time groups.

Protection of spectral degeneracy.—The intertwined space-time symmetries besides translations can protect spectral degeneracies. Below, we consider the effects from the Kramers symmetry without spin and the nonsymmorphic symmetries for the $1+1$D and $2+1$D space-time crystals, respectively.

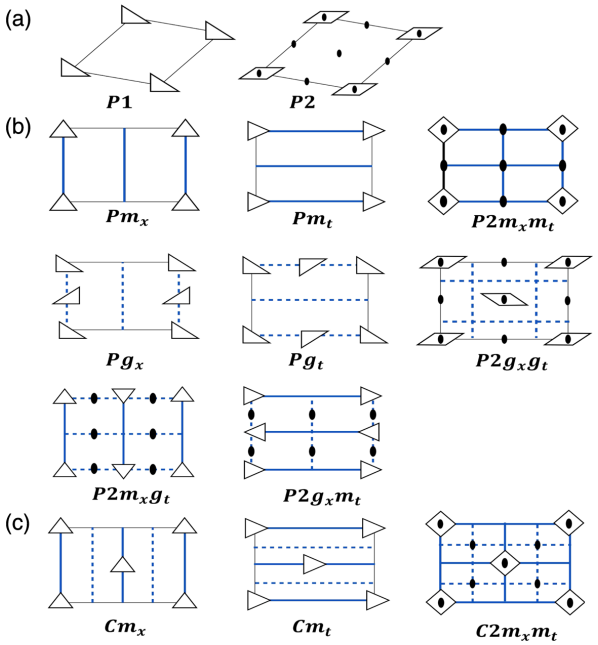

FIG. 2. The classification of 13 space-time groups in $1+1$D and the associated crystal configurations. The solid oval marks the twofold space-time axis, and the parallelogram represents the twofold axis without reflection symmetries. The thick solid and dashed lines represent reflection and glide-reflection axes, respectively. Configurations of the triangles and the diamond denote the local symmetries under reflections. (a) The oblique lattices with and without twofold axes. Their basis vectors are generally space-time mixed. (b) Primitive and (c) centered orthorhombic lattices. According to their reflection and glide reflection symmetries, the crystal configurations are classified into eight groups in (b), and three groups in (c).

Consider a $1+1$D space-time crystal whose unit cell is a direct product of spatial and temporal periods λ and T, respectively. We assume that the system is invariant under the glide time-reversal operation $g_t(x,t) = (x+\frac{1}{2}\lambda, -t)$, whose operation on the Hamiltonian is defined as $g_t^{-1}Hg_t = H^*[g_t(x,t)]$. The corresponding transformation M_{g_t} on the Bloch-Floquet wave function $\psi_\kappa(x,t)$ of Eq. (2) is antiunitarily defined as $M_{g_t}\psi_\kappa = \psi^*_\kappa[g_t^{-1}(x,t)]$. This glide time-reversal operation leaves the line of $\kappa_x = \pi/\lambda$ in the MEBZ invariant. M_{g_t} becomes a Kramers symmetry for states with $\kappa_x = \pi/\lambda$,

$$M^2_{g_t}\psi_\kappa = \psi_\kappa(x-\lambda,t) = e^{-i\kappa_x\lambda}\psi_\kappa = -\psi_\kappa, \tag{5}$$

without involving the half-integer spinor structure. It protects the double degeneracy of the momentum-energy quantum numbers of ψ_κ and $M_{g_t}\psi_\kappa$. Hence, the crossing at $\kappa_x = \pi/\lambda$ cannot be avoided, and the dispersion winding numbers along the momentum direction must be even.

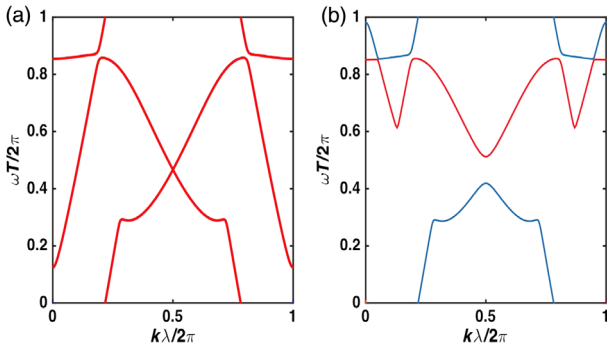

FIG. 3. (a) The Floquet-Bloch band spectrum with the space-time lattice potential possessing the glide time-reversal symmetry g_t. When applied to the states with $\kappa_x = \pi/\lambda$, g_t becomes a Kramers symmetry protecting the double degeneracy. (b) Lifting the Kramers degeneracy by adding a glide time-reversal symmetry breaking term.

As a concrete example, we study a crystal potential with the above spatial and temporal periodicities, $V(x,t) = V_0(\sin[(2\pi)/T]t\cos[(2\pi)/\lambda]x + \cos[(2\pi)/T]t)$. Except for the glide time-reversal symmetry, it does not possess other symmetries. Its Bloch-Floquet spectrum is calculated based on Eq. (3), and a representative dispersion loop is plotted in the MEBZ shown in Fig. 3(a). The crossing at $\kappa_x = \pi/\lambda$ is protected by the glide time-reversal symmetry giving rise to a pair of Kramers doublets. As a result, the winding number of this loop is $\mathbf{w} = (w_x, w_t) = (2,0)$. If a glide time-reversal breaking term $\delta V = V_0' \cos([(2\pi)/\lambda]x)$ is added into the crystal potential, the crossing is avoided, as shown in Fig. 3(b). Consequently, the dispersion splits into two loops, both of which exhibit the winding number (1,0). Similarly, out of the eight primitive orthorhombic space-time crystals, three of them, Pg_t, $P2g_xg_t$, and $P2g_tm_x$, enforce this nonspinor-type Kramers degeneracy, while the other five generally do not protect against such a degeneracy.

Next, we present a $2+1$D Floquet semimetal state whose spectral degeneracies are protected by nonsymmorphic space-time group operations. Consider that the space-time little group of the momentum $\mathbf{k}$ contains two nonsymmorphic space-time group operations $g_{1,2}$, both of which do not flip the time direction; hence, they are represented by unitary operators. If they satisfy

$$g_1 g_2 = T g_2 g_1, \tag{6}$$

where T is a translation of integer lattice vectors. As shown in Sec. IV of the SM [30], T can be a spatial translation only by not involving the time, denoted as $T(\mathbf{u})$. Assuming $\mathbf{k}\cdot\mathbf{u} = 2\pi p/q$, with p and q being coprime, we find that the Bloch-Floquet wave functions exhibit a q-fold degeneracy at the momentum-energy vector $\kappa = (\mathbf{k}, \omega)$, which is proved as follows. Since g_1 belongs to the little group, $\psi_\kappa(\mathbf{r}, t)$ can be chosen to satisfy $M_{g_1}\psi_{\kappa,1} = \mu\psi_{\kappa,1}$, in which case ψ_κ, $M_{g_2}\psi_\kappa, M_{g_2}^2\psi_\kappa, \ldots, M_{g_2}^{q-1}\psi_\kappa$ are the common Bloch-Floquet eigenstates sharing the same κ but exhibiting a set of different eigenvalues of g_1: $\eta, \mu\eta, \mu\eta^2, \ldots, \mu\eta^{q-1}$, with $\eta = e^{i\pi p/q}$. They are then orthogonal to each other, forming a q-fold degeneracy. Compared to the case of a nonsymmorphic space group protected degeneracy [23,24,27], here $g_{1,2}$ are space-time operations for a dynamic space-time crystal. For the case in which one or both $g_{1,2}$ values flip the time direction, the situation is more involved due to the involvement of antiunitary operations. Protected degeneracies are still possible, as presented in Sec. IV of the SM [30].

We employ a $2+1$D tight-binding space-time model as an example to illustrate the above protected degeneracy. A snapshot of the lattice is depicted in Fig. 4(a), which consists of two sublattices: The A-type sites are with integer coordinates (i,j), and each A site emits four bonds along $\vec{e}_i$ to its four neighboring B sites at $(i \pm \frac{1}{2}, j \pm \frac{1}{2})$. The space-time Hamiltonian within the period T is

$$H(t) = -\sum_{\vec{r}\in A, \vec{r}+\frac{a}{2}\vec{e}_i \in B} \{w_{\vec{e}_i}(t) c_{\vec{r}}^\dagger d_{\vec{r}+\frac{a}{2}\vec{e}_i} + \text{H.c.}\}, \tag{7}$$

where a is the distance between the two nearest A sites, and the $w_{\vec{e}_i}(t)$ values are hopping amplitudes with different strengths. Their time dependence is illustrated in Fig. 4(b): Within each quarter period, $w_{\vec{e}_i}$ does not vary, and the

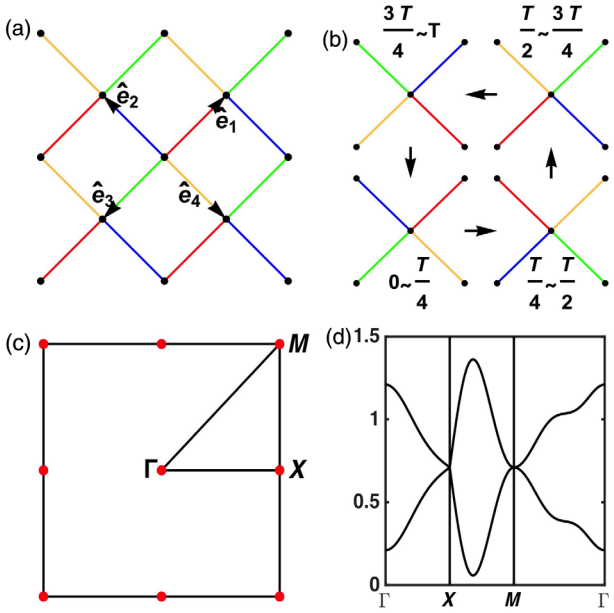

FIG. 4. (a) The $2+1$D space-time lattice structure of the Hamiltonian equation (7). The bond directions are indicated as $\vec{e}_{1,3} = \pm\frac{1}{2}(\hat{x}+\hat{y})$ and $\vec{e}_{2,4} = \mp\frac{1}{2}(\hat{x}-\hat{y})$. (b) The time-dependent hopping pattern rotates 90° every one quarter period. The bonding strengths $w_{e_i}(t)$ of the R, B, G, and Y bonds equal 0.2, 3, −3.2, and 0.5, respectively. (c) The momentum Brillouin zone with high symmetry points $\Gamma = (0,0)$, $M = (\pm\pi, \pm\pi)$, and $X = (0, \pm\pi)$ and $(\pm\pi, 0)$. (d) The dispersions along the cuts from Γ to X to M to Γ. Twofold degeneracies appear at X and M.

pattern rotates 90° after every $T/4$ period. At each given time, the lattice possesses a simple 2D space group symmetry $p2111$, which includes only twofold rotations around the AB-bond centers without reflection and glide-plane symmetries. For example, the rotation R_π around $((a/4),(a/4))$ transforms the coordinate $(x,y,t) \to ((a/2)-x,(a/2)-y,t)$. In addition, there exist time-screw operations—say, an operation S defined as a rotation around an A site (0,0) at 90° followed by a time translation at $T/4$, which transforms $(x,y,t) \to (y,-x,t+(T/4))$. R_π and S are generators of the space-time group for the Hamiltonian equation (7). Since S is a time-screw rotation, this space-time group is nonsymmorphic. It is isomorphic to the 3D space-group $I4_1$, while its 2D space subgroup $p2111$ is symmorphic. We have checked to ensure that, for a static Hamiltonian having the bond configuration shown in Fig. 4(b), the energy spectra are fully gapped. However, the nonsymmorphic space-time group gives rise to spectral degeneracies. Its momentum Brillouin zone is depicted in Fig. 4(c). The space-time little group of the M point (π,π) contains both R and S, satisfying $RS = T(a\hat{y})SR = -SR$. Similarly, the X point $(\pi,0)$ is invariant under both R and S^2, satisfying $RS^2 = T(a\hat{x}+a\hat{y})S^2R = -S^2R$. Hence, the Floquet eigenenergies are doubly degenerate at the M and X points, as shown in Fig. 4(d), showing a semimetal structure.

In conclusion, we have studied a novel class of $(D+1)$-dimensional dynamic crystal structures exhibiting the general space-time periodicities. Their MEBZs are $(D+1)$-dimensional tori and are typically momentum-energy entangled. The band dispersions exhibit nontrivial windings around the MEBZs. The space-time crystal structures are classified by space-time group, which extends the space group for static crystals by incorporating time-screw rotations and time-glide reflections. In $1+1$D, a complete classification of the 13 space-time groups is performed, and there exist 275 space-time groups in $2+1$D. Space-time symmetries give rise to a novel Kramers degeneracy independent of the half-integer spinor structure. The nonsymmorphic space-time group operations lead to protected spectral degeneracies for space-time crystals. This Letter sets up a symmetry framework for exploring the novel properties of space-time crystals. It also serves as the starting point for future studies, for example, dynamical topological phases of matter based on their space-time groups.

This work is supported by the Air Force Office of Scientific Research under Grant No. FA9550-14-1-0168. We also acknowledge the partial support from the National Natural Science Foundation of China under Grant No. 11729402.

Note added.—Recently, we noticed an interesting and important work by T. Morimoto *et al.* [34] classifying Floquet topological crystalline insulators with twofold space-time symmetries.

[1] M. Z. Hasan and C. L. Kane, Rev. Mod. Phys. **82**, 3045 (2010).
[2] X.-L. Qi and S.-C. Zhang, Rev. Mod. Phys. **83**, 1057 (2011).
[3] C. K. Chiu, J. C. Y. Teo, A. P. Schnyder, and S. Ryu, Rev. Mod. Phys. **88**, 035005 (2016).
[4] T. Oka and H. Aoki, Phys. Rev. B **79**, 081406 (2009).
[5] Z. Gu, H. A. Fertig, D. P. Arovas, and A. Auerbach, Phys. Rev. Lett. **107**, 216601 (2011).
[6] N. H. Lindner, G. Refael, and V. Galitski, Nat. Phys. **7**, 490 (2011).
[7] G. Jotzu, M. Messer, R. Desbuquois, M. Lebrat, T. Uehlinger, D. Greif, and T. Esslinger, Nature (London) **515**, 237 (2014).
[8] M. C. Rechtsman, J. M. Zeuner, Y. Plotnik, Y. Lumer, D. Podolsky, F. Dreisow, S. Nolte, M. Segev, and A. Szameit, Nature (London) **496**, 196 (2013).
[9] D. Leykam, M. C. Rechtsman, and Y. D. Chong, Phys. Rev. Lett. **117**, 013902 (2016).
[10] T. Kitagawa, E. Berg, M. Rudner, and E. Demler, Phys. Rev. B **82**, 235114 (2010).
[11] J. K. Asbóth, B. Tarasinski, and P. Delplace, Phys. Rev. B **90**, 125143 (2014).
[12] R. Roy and F. Harper, Phys. Rev. B **96**, 155118 (2017).
[13] M. Thakurathi, A. A. Patel, D. Sen, and A. Dutta, Phys. Rev. B **88**, 155133 (2013).
[14] J. C. Budich, Y. Hu, and P. Zoller, Phys. Rev. Lett. **118**, 105302 (2017).
[15] M. S. Rudner, N. H. Lindner, E. Berg, and M. Levin, Phys. Rev. X **3**, 031005 (2013).
[16] P. Titum, E. Berg, M. S. Rudner, G. Refael, and N. H. Lindner, Phys. Rev. X **6**, 021013 (2016).
[17] A. C. Potter and T. Morimoto, Phys. Rev. B **95**, 155126 (2017).
[18] A. C. Potter, T. Morimoto, and A. Vishwanath, Phys. Rev. X **6**, 041001 (2016).
[19] C. W. von Keyserlingk and S. L. Sondhi, Phys. Rev. B **93**, 245145 (2016).
[20] C. W. von Keyserlingk and S. L. Sondhi, Phys. Rev. B **93**, 245146 (2016).
[21] D. V. Else and C. Nayak, Phys. Rev. B **93**, 201103 (2016).
[22] L. Fu, Phys. Rev. Lett. **106**, 106802 (2011).
[23] S. A. Parameswaran, A. M. Turner, D. P. Arovas, and A. Vishwanath, Nat. Phys. **9**, 299 (2013).
[24] S. M. Young and C. L. Kane, Phys. Rev. Lett. **115**, 126803 (2015).
[25] Z. Wang, A. Alexandradinata, R. J. Cava, and B. A. Bernevig, Nature (London) **532**, 189 (2016).
[26] J. Kruthoff, J. de Boer, J. van Wezel, C. L. Kane, and R.-J. Slager, Phys. Rev. X **7**, 041069 (2017).
[27] H. Watanabe, H. C. Po, M. P. Zaletel, and A. Vishwanath, Phys. Rev. Lett. **117**, 096404 (2016).
[28] B. Bradlyn, L. Elcoro, J. Cano, M. G. Vergniory, Z. Wang, C. Felser, M. I. Aroyo, and B. Andrei Bernevig, Nature (London) **547**, 298 (2017).
[29] A. Bouhon and A. M. Black-Schaffer, Phys. Rev. B **95**, 241101 (2017).

[30] See Supplemental Material at http://link.aps.org/supplemental/10.1103/PhysRevLett.120.096401, which includes Refs. [31–33], for further explanations and additional technical details.

[31] *International Tables for Crystallography, Volume C: Mathematical, Physical and Chemical Tables*, edited by E. Prince (International Union of Crystallography, Chester, England, 2004).

[32] H. Hiller, Am. Math. Mon. **93**, 765 (1986).

[33] *International Tables for Crystallography, Volume A: Space-Group Symmetry*, edited by M. I. Aroyo (International Union of Crystallography, Chester, England, 2016).

[34] T. Morimoto, H. C. Po, and A. Vishwanath, Phys. Rev. B **95**, 195155 (2017).